Mechatronic Design of Hard-Mount Concepts for Precision Equipment

J. van Dijk

Abstract The contribution of the paper is on the conceptual design of mounts, using MiMo state space models describing the spatial flexible multibody system dynamics. Furthermore the contribution is on the evaluation of acceleration feedback versus force-feedback of a hard-mounted metrology frame suspension of a photolithography machine. It includes the modal decoupling controller design. It will be shown that from a vibration energy flow point of view the use of acceleration sensors are preferred.

1 Introduction

The paper deals with the mechatronic design of hard-mounts for vibration isolation in precision equipment. The contribution of the paper is on conceptual design using adequate MiMo state space models describing the spatial system dynamics and the evaluation of acceleration feedback versus force-feedback. The conceptual design, including the modal decoupling controller design, for mounts for a metrology frame suspension of a lithography machine (waver-stepper) is outlined.

Usually precision equipment is mounted on soft-mounts to provide disturbance rejection from base vibrations. For this purpose the suspension resonance frequencies are designed to be low (1 Hz). However, the use of soft-mounts may lead to dynamic instability for equipment with a relatively high center of gravity [1]. Another approach is to use hard-mounts [2]. They provide a stiffer support and as a consequence the suspension resonance frequencies are increased (10–20 Hz). In the case of hardmounts the transmissibility of base vibrations is actively reduced, using sensors, actuators and a control system.

J. van Dijk
Mech. Automation and Mechatronics Laboratory, Faculty of Engineering Technology, University of Twente, Enschede, The Netherlands; E-mail: j.vandijk@ctw.utwente.nl

H. Ulbrich and L. Ginzinger (eds.), Motion and Vibration Control, 315–324.

The metrology frame provides the support for the optical device (lens). The lens and the frame are considered rigid in the frequency region of interest (0–300 Hz). But due to the their flexible connection the frame-lens combination has internal modes in the region 80–100 Hz [3]. The idea is to design a hybrid-elastic mount with a high stiffness (typically 200–400× higher than for pneumatic isolators). The hard-mount concept discussed is based on an elastic structure and includes per mount 2 piezo-actuators. Three mounts will be used to support the metrology frame.

For evaluation of conceptual designs it is important to model the spatial system dynamics of the equipment and to obtain Multiple input and Multiple output transfer-matrices or state space descriptions. To obtain these MiMo models can be a tedious task [1]. The multibody system approach is a well-suited method to model the spatial dynamic behavior. In this approach the mechanical components are considered as rigid or flexible bodies that interact with each other through a variety of connections such as hinges and flexible coupling elements.

An implementation of this method is realized in the program `SPACAR` [4], [5] which has an interface to `MATLAB`. The method to obtain state space descriptions with this program is based on a nonlinear finite element description for multibody systems and accounts for geometric nonlinear effects of flexible elements due to axial and transverse displacements. This modelling approach is applied to the described setup in Section 2.

In Section 3 we evaluate the transmissibility from base-vibrations to internal mode excitation. This is not common, but this is the effective transmissibility that can jeopardize the accuracy of the device. In Section 4 the controller design based on modal decoupling is described. In Section 5 we evaluate, using the obtained MiMo state space models, the pros and cons of force feedback as well as acceleration feedback. It will be shown that from a vibration energy flow point of view acceleration sensors are preferred despite the fact that with these type of sensors co-located control is not guaranteed [6]. Therefore, this conclusion is contradictive to the conclusion drawn by Preumont et al. [6] but is drawn from a different viewpoint. It will also be shown that force sensors can be used if special specifications of the mechanical structure of the mounts are realized.

2 Modelling

Structural systems have dynamics which in linearized form can be described by ordinary differential equations of the following form:

$$M\ddot{\boldsymbol{q}} + D\dot{\boldsymbol{q}} + K\boldsymbol{q} = \boldsymbol{f} \tag{1}$$

where M, D and K are the usual mass, damping and stiffness matrix, $\boldsymbol{f}$ is the vector of applied generalized forces. The vector $\boldsymbol{q}$ is used to denote the generalized displacement vector or degrees of freedom. In [5] it is shown that in case of driving terms which are not solely forces but are also rheonomic displacements or their time

Table 1 Inertia properties of the frame and lens and equivalent stiffness properties of a leg.

	Mass [kg]	I_{xx} [kg/m^2]	I_{yy} [kg/m^2]	I_{zz} [kg/m^2]
frame	742	52.25	52.25	104.5
lens	851.6	72.95	72.95	49.15
length m	long. stiffn.	bend. stiffn. y	bend. stiffn. z	torsional stiffn.
0.283	$8.389 \cdot 10^6$ N/m	371 Nm	371 Nm	5.84Nm

derivatives, (1) changes to the form:

$$M_d \cdot \ddot{\boldsymbol{q}}_d + D_d \cdot \dot{\boldsymbol{q}}_d + K_d \cdot \boldsymbol{q}_d = -M_r \cdot \ddot{\boldsymbol{q}}_r + B_0 \cdot \sigma_a \tag{2}$$

where M_d, D_d and K_d are the mass, damping and stiffness matrix corresponding with the degrees of freedom $\boldsymbol{q}_d$ and M_r is the mass-matrix corresponding with the rheonomic degrees of freedom $\boldsymbol{q}_r$. B_0 describes the location of the actuator-forces σ_a with respect to the degrees of freedom. The restriction at (2) is that the degrees of freedom $\boldsymbol{q}_d$ are chosen as a vector of relative displacements.

The control theory uses often systems of first-order differential equations written in state space form:

$$\dot{\boldsymbol{x}} = A \cdot \boldsymbol{x} + B \cdot \boldsymbol{u} \tag{3}$$

$$\boldsymbol{y} = C \cdot \boldsymbol{x} + D \cdot \boldsymbol{u} \tag{4}$$

$$u = H \cdot y \tag{5}$$

where $\boldsymbol{y}$ is the vector of sensor output signals, C is the output matrix and D the feed-through matrix. The vector $\boldsymbol{x}$ is called the state-vector. Output feedback is described by (5), where H is a frequency dependent gain matrix to satisfy some performance. The relationship between the physical coordinate description given by (2) and the state equations (3) is:

$$A = \begin{bmatrix} \boldsymbol{O} & \boldsymbol{I} \\ -M_d^{-1} K_d & -M_d^{-1} D_d \end{bmatrix}, B = \begin{bmatrix} \boldsymbol{O} \\ M_d^{-1}[-M_r, B_0] \end{bmatrix}, \boldsymbol{x} = \begin{bmatrix} \boldsymbol{q}_d \\ \dot{\boldsymbol{q}}_d \end{bmatrix}, \boldsymbol{u} = \begin{bmatrix} \sigma_a \\ \ddot{\boldsymbol{q}}_r \end{bmatrix} \tag{6}$$

where $-M_d^{-1} M_r = T_u$ is a coordinate transformation.

Based on the extended representation as in (2), state space descriptions of the metrology frame for analyses and active vibration control will be obtained using a flexible multibody system approach as described in [5]. Table 1 gives an overview of the inertia properties of the frame and lens. The moments of inertia I_{xx}, I_{yy} and I_{zz} are defined with respect to the center of gravity of the frame and lens respectively.

The frame is supported by mounts. Each mount consists of two legs which will be modelled by simple flexible beam like structures. These flexible beams represent the equivalent stiffness properties of the mount. The beam element is modelled as an active element which provides for the passive elastic properties of the leg and the

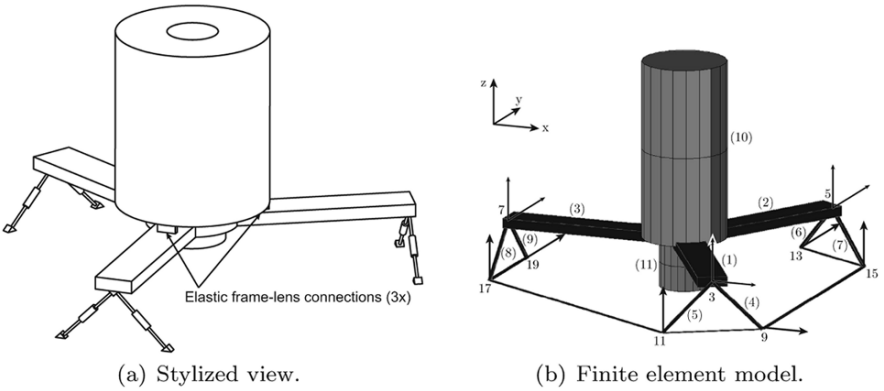

(a) Stylized view. (b) Finite element model.

Fig. 1 Stylized view and FEM-model using beams of lens suspension frame of a wafer stepper/scanner.

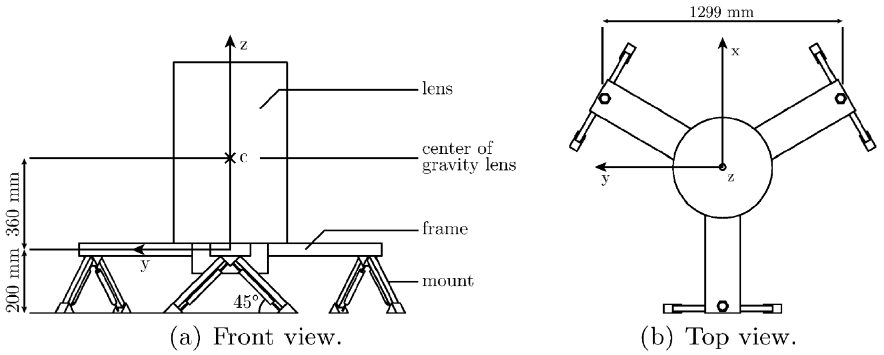

(a) Front view. (b) Top view.

Fig. 2 Front and top view of the metrology frame.

longitudinal force of the piezo actuator. Table 1 shows the stiffness properties of the elastic beam elements.

The metrology frame is modelled using 20 spatial beam elements numbered (1) to (20) and hereafter simply called beams, see Figure 1(b). The beams (1), (2), (3), (12), (13), (14) represent the frame. The beams (10) and (11) represent the lens. The connection between frame and lens is modelled using 6 beams, beams (15), (16), (17), (18),(19) and (20). Beam-elements (1), (2), (3), (10) (11), (12), (13), (14), (18), (19) and (20) are rigid. The inertia properties of the rigid beams match the inertia properties of frame and lens as in Table 1. Beams (4), (5), (6), (7), (8) and (9) represent the active-elastic beams of the mounts and beams (15), (16) and (17) represent the flexible connection blocks between frame and lens. All flexible beams are considered mass-less with respect to the heavy frame and lens.

As dynamic degrees of freedom we choose the longitudinal deformations of the suspension beams constituting the legs ($\boldsymbol{q}_s$) and the deformations of one element

representing a flexible connection blocks ($\boldsymbol{q}_i$) i.e.

$$\boldsymbol{q}_d = \left[e_1^{(4)}, e_1^{(5)}, e_1^{(6)}, e_1^{(7)}, e_1^{(8)}, e_1^{(9)}, e_1^{(15)}, e_2^{(15)}, e_3^{(15)}, e_4^{(15)}, e_5^{(15)}, e_6^{(15)}\right]^T \tag{7}$$

where the numbers between the brackets denote the element numbers and the subscripts denote the deformation direction.

The base is modelled as a rigid body configuration built-up by means of rigid beam elements. Because we are interested in the open loop and later on also in the closed loop transfer functions between base vibration and frame vibrations, the base excitations are defined as rheonomic accelerations applied at the nodal points between legs and base as shown in Figure 1(b). They are defined by the input vector (8), where the superscript numbers represent the associated node numbers, see Figure 1(b).

$$\boldsymbol{u}^{(\text{floor})} = \left[\ddot{x}^9, \ddot{z}^{11}, \ddot{y}^{13}, \ddot{z}^{15}, \ddot{z}^{17}, \ddot{y}^{19}\right]^T, \tag{8}$$

$$\boldsymbol{u}^{(\text{actuator})} = \left[\sigma_a^{(4)}, \sigma_a^{(5)}, \sigma_a^{(6)}, \sigma_a^{(7)}, \sigma_a^{(8)}, \sigma_a^{(9)}\right]^T. \tag{9}$$

$$\boldsymbol{y}^{(\text{frame-lens})} = \left[\ddot{e}_1^{(15)}, \ddot{e}_2^{(15)}, \ddot{e}_3^{(15)}, \ddot{e}_4^{(15)}, \ddot{e}_5^{(15)}, \ddot{e}_6^{(15)}\right]^T \tag{10}$$

$$\boldsymbol{y}^{(\text{force})} = \left[\sigma_1^{(4)}, \sigma_1^{(5)}, \sigma_1^{(6)}, \sigma_1^{(7)}, \sigma_1^{(8)}, \sigma_1^{(9)}\right]^T \tag{11}$$

$$\boldsymbol{y}^{(\text{frame})} = \left[\ddot{x}^3, \ddot{z}^3, \ddot{y}^5, \ddot{z}^5, \ddot{z}^7, \ddot{y}^7\right]^T \tag{12}$$

The input vector of actuator forces, associated with the active beams numbered (4)–(9) are defined by (9).

The outputs are defined in two parts as well. The first part contains the output-signals of so-called virtual performance acceleration sensors which measure the relative acceleration between lens and frame in element number (15). These accelerations are included in the output vector as described by (10). The second part contains the feedback sensors. Which are in the case of force-control the outputs of force sensors described by (11). These sensors measure the longitudinal stress resultant $\sigma_1^{(k)}$ of the elastic beams, i.e. the actuator forces summed with the normal forces due to the elongation of the elastic beams. In the case of acceleration feedback control they are the accelerations of the frame in the nodal points 3, 5 and 7. The feedback accelerations are included in the output vector (12).

3 Mode-Shape and Singular Value Analyses of the Model

Figure 3 shows the result of the mode-shape analysis. The figure shows the shapes and corresponding frequencies of the suspension modes in which the lens and frame behave as a rigid body. From Figure 3 it can be concluded that the fourth, fifth and

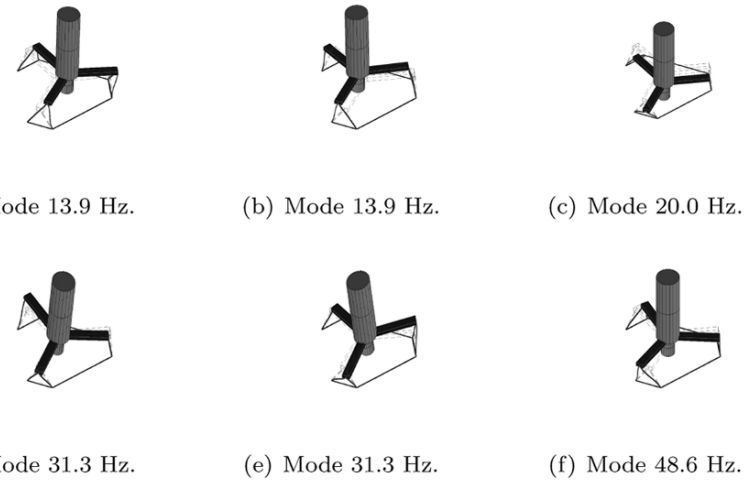

(a) Mode 13.9 Hz. (b) Mode 13.9 Hz. (c) Mode 20.0 Hz.

(d) Mode 31.3 Hz. (e) Mode 31.3 Hz. (f) Mode 48.6 Hz.

Fig. 3 Mode shapes and natural frequencies of the suspension modes.

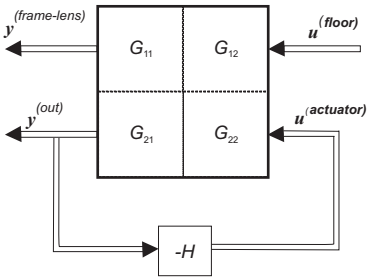

Fig. 4 Generalised plant $\boldsymbol{G}$ with 12 inputs and 12 outputs and controller $\boldsymbol{C}$ with 6 inputs and 6 outputs.

sixth mode are two high frequent. It takes quite some actuator force to bring these modes back to 1 Hz in the closed loop (active) case. As a consequence one has to design the lens-support frame with a smaller basis. The consequence of a smaller basis is a decrease in tilt- and torsional stiffness.

Figure 4 shows the 12×12 generalised plant $\boldsymbol{G}$ with the in- and output vectors defined by Eqs. (8) to (12). Matrix $\boldsymbol{G}$ is partitioned in four transfer matrices $\boldsymbol{G}_{11}, \boldsymbol{G}_{12}, \boldsymbol{G}_{21}$ and $\boldsymbol{G}_{22}$. Of interest are the singular values of the open loop transfer matrix $\boldsymbol{G}_{11}$ between base accelerations and the performance accelerations. The singular values represent the principle gains of the transfer matrix. Especially the largest singular value is important because it shows the worst-case gain frequency relationship between an input and an output vector of the given input and output set. Therefore, in the open loop case this largest singular value gives an impression of the passive vibration isolation. Figure 5(a) shows the largest singular value versus frequency (solid line) of the transfer function $\boldsymbol{G}_{11}$. From this figure we can conclude

that in the frequency region of the internal modes the transmissibility is close to one. Assuming the base vibrations as white noise, Figure 5(a) indicates that the internal modes are excited by the base vibrations.

4 Controller Design

In order to provide isolation of base vibrations from 1 Hz and beyond and to provide sufficient artificial damping of the suspension modes additional control forces $\boldsymbol{u}^{(\text{actuator})}$ are applied. These forces are computed on the basis of six accelerations, defined in $y^{(\text{frame})}$ (12), or force output signals $y^{(\text{force})}$ (11). The control strategy is to combine proportional and integral feedback. This is equivalent with adding virtual mass, which lowers the frequencies of the suspension modes and adding artificial damping respectively.

The assumptions are the following. The system is considered rigid (no internal modes) for the control design. Then there are 6 modelled modes. $n = 6$ *relative* degrees of freedom ($\boldsymbol{q}_s = [e_1^{(4)}, e_1^{(5)}, e_1^{(6)}, e_1^{(7)}, e_1^{(8)}, e_1^{(9)}]^T$) have been chosen for modelling. Demping can be neglected. The equations of motion (2) are then written as:

$$M_d \cdot \ddot{\boldsymbol{q}}_s + K_d \cdot \boldsymbol{q}_s = -M_r \cdot \ddot{\boldsymbol{q}}_r + B_0 \cdot \sigma_a \tag{13}$$

First we use proportional acceleration and integral acceleration feedback.

$$\sigma_a = -K_a \cdot y^{(\text{frame})} - K_v \cdot \dot{Y} \tag{14}$$

in which $\dot{Y}$ is the integral of the n accelerometer outputs ($y^{(\text{frame})}$). Equation (14) can be rewritten as:

$$\begin{aligned} \sigma_a &= -K_a \cdot T_c \cdot \ddot{\boldsymbol{q}}_s - K_v \cdot T_c \cdot \dot{\boldsymbol{q}}_s \\ &= -K'_a \cdot \ddot{\boldsymbol{q}}_s - K'_v \cdot \dot{\boldsymbol{q}}_s \end{aligned} \tag{15}$$

in which T_c is some constant geometrical transformation between the degrees of freedom $\boldsymbol{q}_s$ and the positions Y of the accelerometers. Substitution of (15) into (13) results in:

$$M_d \cdot \ddot{\boldsymbol{q}}_s + K_d \cdot \boldsymbol{q}_s = -M_r \cdot \ddot{\boldsymbol{q}}_r + B_0 \cdot (-K'_a \cdot \ddot{\boldsymbol{q}}_s - K'_v \cdot \dot{\boldsymbol{q}}_s) \tag{16}$$

Using a modal decoupling appoach [7], Eq. (16) can be rewritten in decoupled form as:

$$(I_n + S' B_0 K'_a S)\ddot{z} + S' B_0 K'_v S\dot{z} + S' K_d S z = -S' M_r \ddot{q}_r \tag{17}$$

in which I_n is the $n \times n$ identity matrix, $S = M_d^{-1/2} \cdot P$ and P is the matrix whose columns are the normalized eigenvectors of $M_d^{-1/2} K_d M_d^{-1/2}$. The left-hand side of (17) is decoupled. Equation (17) is obtained after a succesive substitution of $\boldsymbol{q} = M_d^{-1/2} \underline{\mathrm{r}}$ and $\underline{\mathrm{r}} = P \cdot z$. Without constraints it can be stated that the new

modal mass-matrix $(I_n + S' B_0 K'_a S)$ should yield (remark that all these matrices are diagonal matrices):

$$(I_n + S' B_0 K'_a S) = \frac{1}{\omega_n^2} \cdot S' K_d S \tag{18}$$

where ω_n is the desired corner frequency and therefore:

$$\begin{aligned} K'_a &= B_0^{-1} \frac{1}{\omega_n^2} \cdot K_d - B_0^{-1} M_d \\ K_a &= K'_a \cdot T_c^{-1} \end{aligned} \tag{19}$$

We define also the following:

$$\begin{aligned} S' B_0 K'_v S &= 2\zeta_n \omega_n \cdot (S' B_0 K'_a S + I_n) \\ K'_v &= B_0^{-1} \cdot 2\zeta_n \omega_n \cdot (B_0 K'_a + M_d) \\ K_v &= K'_v \cdot T_c^{-1} \end{aligned} \tag{20}$$

where ζ_n is the desired relative damping. In here the actuators are delivering forces in the direction of the degrees of freedom, therefore $B_0 = I_n$. The consequence of (19) and (20) is that the acceleration feedback controller is defined by

$$H_{\text{acc}}(s) = -\left(K_a + K_v \cdot \frac{1}{s}\right) \tag{21}$$

Application of an equivalent approach results in the force feedback controller to read:

$$\begin{aligned} K_P &= (\omega_n^2 \cdot I_n \cdot M^{dd})^{-1} \cdot K^{dd} - I_n \\ K_I &= 2\zeta\omega_n \cdot (I_n + K_P) \\ H_f(s) &= -\left(K_P + K_I \cdot \frac{1}{s}\right) \end{aligned} \tag{22}$$

In case of force-sensing the sensing is also in the direction of the defined degrees of freedom making the matrix T_c the identity-matrix.

5 Evaluation of Acceleration versus Force Feedback

Figure 5(a) shows a plot of the largest singular value of the open and closed loop transfer function matrix between base and internal mode accelerations. The closed loop is either established by force feedback (dashed line) or by acceleration feedback (dotted line). It can be observed that the natural frequencies of all suspension modes are brought back to 1 Hz by active means and that the suspension modes are well damped. In the case of acceleration feedback the internal modes are lowered in frequency and still undamped but the excitation is reduced 50 dB in magnitude. The decrease in frequency of the internal modes can be understood from the following.

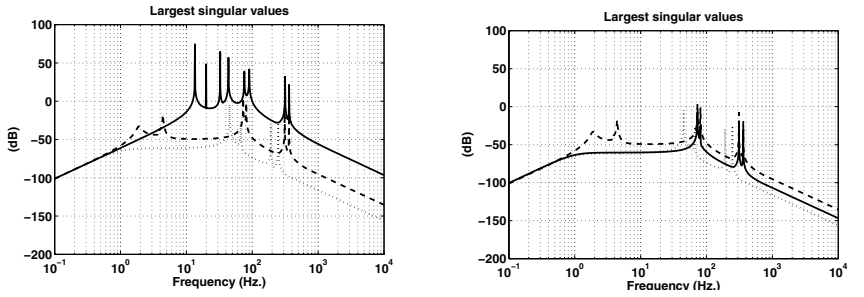

(a) (b)

Fig. 5 (a) Open loop (solid), acc. feedback (dotted), force feedback (dashed), (b) acc. feedback (dotted), force feedback (dashed), low parasitic stiffness force feedback (solid).

The transfers between actuators and sensors, usually called secondary path, contains zeros. There is no control at the frequencies of the zeros, with the consequence that new resonances appear at the frequencies of these zero dynamics. The zero dynamics of the secondary path transfer, are determined by the dynamics in case the sensors are blocked (zero output of acceleration sensors). As a consequence, these zero dynamics correspond with the internal mode dynamics in case the frame is not moving. These dynamics are lower in frequency then the frequencies of the internal modes in the uncontrolled case. Therefore, in the acceleration feedback control case the new internal mode frequencies correspond with the frequencies of the zeros in the secondary path transfers.

In case of force feedback, Figure 5(a) shows that there is less reduction in excitation of the internal modes by base-vibration compared to the acceleration feedback case. This is due to the fact that the sensors are only capable of measuring forces in longitudinal direction in the legs. Forces transmitted to the frame by bending and torsion are not measured. This force distribution through these so called parasitic paths can be analyzed again by analyses of the zeros in the secondary path. Since these zero dynamics, in the case of force feedback, are determined in the situation where the sensor outputs are zero. This is the case if the actuator forces compensate the stiffness in longitudinal direction. The zero dynamics are then described by the residual system dynamics where the longitudinal stiffnesses are set to zero. Say we make these zero dynamics have passive behavior below the specification of 1 Hz. Then, the performance in the controlled case is better. See Figure 5(b) (solid line) for the result of lowering the bending and torsional stiffness to the required amount such that the residual dynamics and as a consequence the zero dynamics, have frequencies in the region 0.1 Hz to 0.8 Hz. Overall we can conclude that with acceleration feedback better performance is obtained then with force feedback. Given the fact that in both controlled cases the same corner frequency and damping of the suspension modes is established.

6 Conclusions

Shown is that a flexible multibody modelling approach can give adequate state space models for analysis and conceptual design of vibration isolation systems using hard-mounts. It is shown that using a modal control approach the performance of hard-mounts can be made comparable to the performance of soft-mounts. The advantage is however an increased dynamic stability. When using acceleration feedback a better performance is obtained then when using force feedback. Given that in both controlled cases the same corner frequency and damping of the suspension modes is established.

References

1. M. Heertjes and K. de Graaff. Active vibration isolation of metrology frames; A modal decoupled control design. *ASME Journal of Vibration and Acoustics* **127**, 223–233, 2005.
2. TMC. http://www.techmfg.com. Technical Background, section 5.5 (STACIS).
3. J. Holterman. *Vibration Control of High-Precision Machines with Active Structural Elements*. PhD thesis, Twente University Press, University of Twente, Enschede, The Netherlands, 2002.
4. J.B. Jonker and J.P. Meijaard. SPACAR-computer program for dynamic analysis of flexible spational mechanisms and manipulators. In: *Multibody Systems Handbook*, W. Schiehlen (Ed.), pp. 123–143. Springer-Verlag, Berlin, 1990.
5. J.B. Jonker, R.G.K.M. Aarts, and J. van Dijk. An extended input-output representation for control synthesis in multibody system dynamics. In: *Proc. 2007 Eccomas Multibody 2007*, Milano, Vol. 53, pp. 208–215, 2007.
6. A. Preumont, A. Francois, F. Bossens, and A. Abu-Hanieh. Force feedback versus acceleration feedback in active vibration isolation. *Journal of Sound and Vibration* **257**(4), 605–613, 2002.
7. D.J. Inman. Active modal control for smart structures. *Philosophical Transactions/Royal Society of London Series A* **359**, 205–219, 2001.